Role of spontaneously transferred coherence in laser cooling

Rajnandan Choudhury Das, Thilagaraj Ravi, Samir Khan, and Kanhaiya Pandey*
Department of Physics, Indian Institute of Technology Guwahati, Guwahati, Assam 781039, India

(Received 8 February 2024; accepted 20 August 2024; published 3 September 2024)

The well-known sub-Doppler polarization gradient cooling in a type-I transition ($F_e = F_g + 1$) is caused by red-detuned lasers. On the other hand, in a type-II transition ($F_e \leqslant F_g$), sub-Doppler cooling takes place through blue-detuned lasers. This opposite behavior for the two types of transitions is due to spontaneously transferred coherence (STC). In the absence of STC, both types of transitions show blue-detuned cooling. In this paper, we experimentally and theoretically demonstrate blue-detuned cooling for both types of transitions in ^{87}Rb. For completeness, we compare the temperatures in various configurations.

DOI: 10.1103/PhysRevA.110.033101

I. INTRODUCTION

Atomic coherence plays a significant role in various interesting phenomena such as electromagnetically induced transparency (EIT) [1–3], electromagnetically induced absorption (EIA) [4,5], and coherent population trapping (CPT) [6,7]. Typically, atomic coherence is destroyed by the spontaneous emission process induced by vacuum electric fields. However, when the same vacuum mode of the electric field simultaneously drives two transitions in a multilevel system, then the spontaneous emission can lead to the buildup of coherence between the ground states through two mechanisms. The first mechanism, known as spontaneously generated coherence (SGC), arises from the decay of the population from the excited state [8–10]. The second, which can be termed spontaneously transferred coherence (STC), results from the transfer of coherence from the excited states to the ground states [11]. For isotropic vacuum electric fields, SGC is not possible between magnetic sublevels due to the orthogonal polarization of the electric fields. However, STC is possible because the same vacuum field (same polarization) can connect the two magnetic sublevels in the excited state (having coherence between them) to the two magnetic sublevels in the ground states. Collectively, these two phenomena are referred to as vacuum-induced coherence (VIC). The role of VIC has been extensively studied in multilevel systems in the context of spectroscopy [12–17]. Since the behavior of laser cooling has a direct connection with the atomic spectrum profile, STC also plays a crucial role in laser cooling.

In alkali atoms, laser cooling is generally realized using type-I transition, i.e., $F_g \rightarrow F_e = F_g + 1$ (where F_g and F_e are the ground- and excited-state angular momenta). In a type-I transition, both Doppler and sub-Doppler cooling require red-detuned lasers [18]. In contrast, for a type-II transition ($F_g \geqslant F_e$), Doppler cooling requires red-detuned lasers, while sub-Doppler cooling requires blue-detuned lasers [19]. The opposite behavior of these two types of transitions is attributed to STC. Red-detuned sub-Doppler cooling is due to the presence of STC which is prominent if the magnetic sublevels are degenerate and is therefore very sensitive to the magnetic field [19–24]. Achieving low temperatures involves carefully nullifying the magnetic field, a task not feasible in the magneto-optical trap (MOT) phase. It is known that blue-detuned cooling occurs in MOT at a type-II transition and has been demonstrated in Rb with significant advantages [24–26]. Furthermore, blue-detuned light offers additional advantages in single-atom loading efficiency in the optical tweezer array, as compared to red-detuned light [27,28]. Blue-detuned MOTs have also been demonstrated in molecules and are crucial for cold molecule experiments [29–33]. In this paper, we show that blue-detuned cooling in MOTs is possible even in a type-I transition.

In the experiment, we utilize a narrow open transition in ^{87}Rb for a MOT [34–36], similar to Li [37,38], K [39], Ca [40,41], Sr [42,43], Yb [44,45], Dy [46,47], Er [48–50], Cd [51], Eu [52], etc. The MOT for ^{87}Rb atoms is realized at the $5S_{1/2}, F = 2 \rightarrow 6P_{3/2}, F = 3$ transition at 420 nm, which has a four to five times lower Doppler temperature (34 μK) than the regularly used broad transition at 780 nm. Since the blue transition is open, we observe that the repumper laser plays a crucial role in lowering the temperature of the narrow-line MOT. We observed that the blue-detuned repumper causes further cooling in both type-I ($F_g = 1 \rightarrow F_e = 2$) and type-II ($F_g = 1 \rightarrow F_e = 1$) transitions in the MOT. We have also explored various other configurations that produce both red-detuned and blue-detuned blue MOTs of Rb.

In this paper, we undertake a comprehensive numerical investigation employing a density matrix analysis to explore the role of STC on the sub-Doppler force in an atomic system characterized by the $F_g = 1 \rightarrow F_e = 2$ transition. Our primary objective is to assess the feasibility of blue-detuned laser cooling in MOT. Subsequently, through experimental exploration, we investigate various configurations of blue-detuned MOTs for Rb at a narrow transition on the D_1 and D_2 lines. Our results, supported by a density matrix analysis, demonstrate the efficacy of blue-detuned laser cooling even in type-I MOTs,

*Contact author: kanhaiyapandey@iitg.ac.in

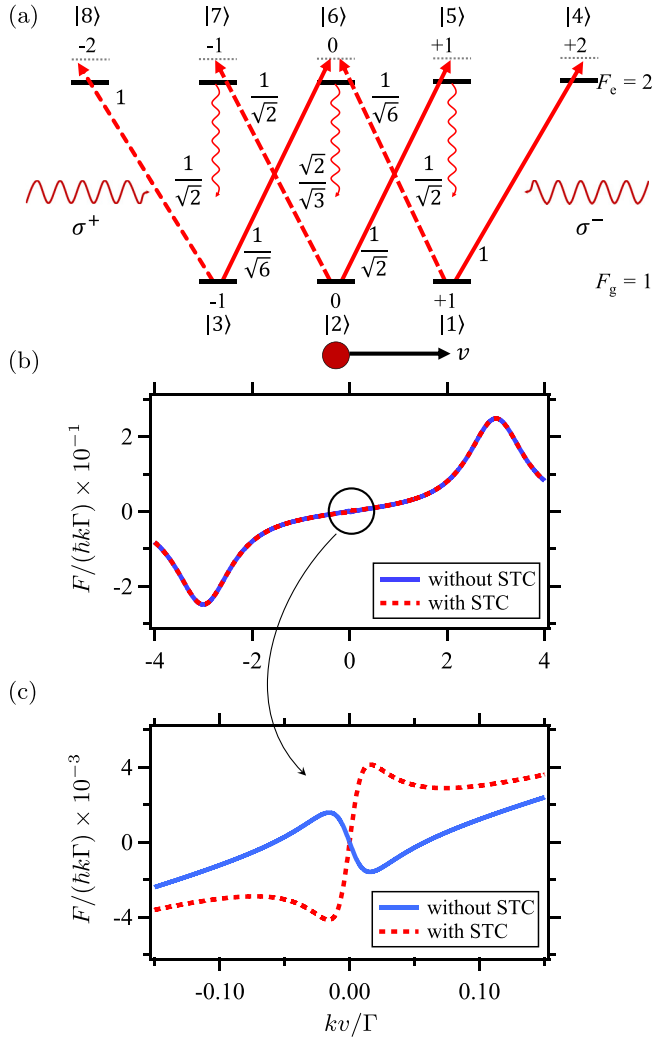

FIG. 1. Effect of $F_g = 1 \rightarrow F_e = 2$. (a) Energy level diagram of the atomic system in the presence of σ^+-σ^- light. Zeeman energy levels are labeled using $|i\rangle$ notation. Clebsch-Gordan coefficients are shown near the transitions. Velocity-dependent force curve for the system is presented for (b) a large velocity range and (c) a small velocity range. The dashed red (solid blue) curve corresponds to the presence (absence) of STC. The black-circled portion in (b) is magnified and illustrated in (c). Parameters: $\Delta_{1\rightarrow 2} = +3\Gamma$ and $\Omega = \Gamma/\sqrt{2}$.

achieving sub-Doppler temperatures as low as 24 μK in the D_1 MOT and 31 μK in the D_2 MOT.

The paper is organized as follows. In Sec. II, we discuss the theoretical framework to study the role of STC in laser cooling using a density matrix analysis. In Sec. III, we discuss the experimental setup. In Sec. IV, we present the results and discussions. Finally, Sec. V is devoted to the conclusions.

II. THEORETICAL FRAMEWORK

First, we analyze the cooling by two counterpropagating lasers with σ^+ and σ^- polarization for $F_g = 1 \rightarrow F_e = 2$ with all the magnetic sublevels [as shown in Fig. 1(a)] using density matrix calculations.

The Hamiltonian H of the eight-level system under the electric-dipole and rotating-wave approximation and in the rotating frame is expressed as

$$H = \hbar\Big\{-2kv|3\rangle\langle 3| + (kv-\Delta)(|4\rangle\langle 4| + |5\rangle\langle 5|) - (kv+\Delta)(|6\rangle\langle 6| + |7\rangle\langle 7|) - (3kv+\Delta)|8\rangle\langle 8| + \frac{1}{2}\Omega\Big(|1\rangle\langle 4| + \frac{1}{\sqrt{6}}|1\rangle\langle 6| + \frac{1}{\sqrt{2}}|2\rangle\langle 5| + \frac{1}{\sqrt{2}}|2\rangle\langle 7| + \frac{1}{\sqrt{6}}|3\rangle\langle 6| + |3\rangle\langle 8|\Big) + \text{H.c.}\Big\}. \quad (1)$$

Here, Δ, Ω, and k denote the detuning, Rabi frequency, and magnitude of the wave vector of the lasers, respectively, and v is the velocity of the atoms. The atom-field interaction is described by writing the Liouville–von Neumann equation for the density matrix,

$$\dot{\rho} = -\frac{i}{\hbar}[H, \rho] + L(\rho). \quad (2)$$

Here, $L(\rho)$ accounts for the spontaneous decay of atoms via various channels. Sixty-four simultaneous differential equations are obtained. Only equations for $\dot{\rho}_{12}$, $\dot{\rho}_{13}$, and $\dot{\rho}_{23}$ have the effect of STC, which are given below. The terms appearing due to STC are underlined:

$$\dot{\rho}_{12} = -\frac{i}{2}\Omega\Big(\rho_{42} + \frac{1}{\sqrt{6}}\rho_{62}\Big) + \frac{i}{2\sqrt{2}}\Omega(\rho_{15}+\rho_{17}) \underline{+\Gamma\Big(\frac{1}{\sqrt{2}}\rho_{45} + \frac{1}{\sqrt{3}}\rho_{56} + \frac{1}{2\sqrt{3}}\rho_{67}\Big)}, \quad (3)$$

$$\dot{\rho}_{13} = -\frac{i}{2}\Omega\Big(\rho_{43} + \frac{1}{\sqrt{6}}\rho_{63}\Big) + \frac{i}{2}\Omega\Big(\frac{1}{\sqrt{6}}\rho_{16} + \rho_{18}\Big) + 2ikv\rho_{13} \underline{+\Gamma\Big(\frac{1}{\sqrt{6}}\rho_{46} + \frac{1}{2}\rho_{57} + \frac{1}{\sqrt{6}}\rho_{68}\Big)}, \quad (4)$$

$$\dot{\rho}_{23} = -\frac{i}{2\sqrt{2}}\Omega(\rho_{53}+\rho_{73}) + \frac{i}{2}\Omega\Big(\frac{1}{\sqrt{6}}\rho_{26} + \rho_{28}\Big) + ikv\rho_{23} \underline{+\Gamma\Big(\frac{1}{2\sqrt{3}}\rho_{56} + \frac{1}{\sqrt{3}}\rho_{67} + \frac{1}{\sqrt{2}}\rho_{78}\Big)}. \quad (5)$$

The remaining equations are presented in the Appendix. They are numerically solved and the force experienced by the atom is evaluated from the absorption of the σ^+ and σ^- light, following a similar approach as in Refs. [18,36,53]. The force on the atom can be given by the following expression,

$$F_{\text{damp}} = \hbar k\Omega\,\text{Im}\Big[(\rho_{14}-\rho_{38}) + \frac{1}{\sqrt{2}}(\rho_{25}-\rho_{27}) + \frac{1}{\sqrt{6}}(\rho_{36}-\rho_{16})\Big]. \quad (6)$$

In Fig. 1(b), we present the force versus velocity plot for a large velocity range under the influence of blue-detuned lasers. The red dashed (blue solid) curve corresponds to the force in the presence (absence) of STC. Both the curves reveal indistinguishable Doppler force profiles for large velocity ranges. Zooming into the black-circled region in Fig. 1(b), Fig. 1(c) provides a closer examination of the small velocity range. STC exerts a substantial influence on the force versus velocity behavior, particularly for lower velocities. In the

presence of STC, atoms with positive (negative) velocities experience a more pronounced positive (negative) force compared to the Doppler force alone, contributing to enhanced heating. Conversely, the absence of STC results in a sign reversal in the slope of the force versus velocity curve, indicating the blue-detuned cooling in a type-I transition. These curves for force versus velocity flip signs for negative detuning, leading to polarization gradient cooling (heating) in the presence (absence) of STC.

The flipping of the sub-Doppler force profile is associated with the absorption from the two counterpropagating lasers by the atom. For the atoms with large velocities, absorption from one laser is not significantly influenced by the other laser and the individual absorption spectrum is Lorentzian. However, for the near-zero velocity group of atoms, the absorption of one laser is modified in the presence of the other laser and the nature of the absorption spectra deviates from the Lorentzian profile for the small velocity range. For the small positive velocity group of atoms, absorption from the σ^+ beam is reduced, due to the presence of the σ^- beam, which is analogous to an EIT dip, and the absorption from the σ^- beam is increased. This is the case in the absence of STC. In the presence of STC, the situation reverses, which is analogous to the conversion of EIT to EIA due to the population redistribution as a result of the STC. Thus, for the same velocity group, absorption from the σ^+ beam is enhanced and that from the σ^- beam is reduced. As a result, the sub-Doppler force profile flips its sign in the presence and absence of STC.

III. EXPERIMENTAL SETUP

The experimental setup comprises one commercially available (Toptica) 420-nm (blue) external cavity diode laser (ECDL) and two home-assembled 780-nm (IR) ECDLs. Polarization spectroscopy is employed for the IR MOT laser's frequency stabilization [34], while saturation absorption spectroscopy is used for the IR repumper laser and the blue laser (similar to our previous experiments [36,54]). Four sets of beams L_1, L_2, L_3, and L_4 are derived which are IR MOT ($5S_{1/2}$, $F = 2 \rightarrow 5P_{3/2}$, $F = 3$), IR repumper ($5S_{1/2}$, $F = 1 \rightarrow 5P_{3/2}$, $F = 1$ or 2), red-detuned blue MOT ($5S_{1/2}$, $F = 2 \rightarrow 6P_{3/2}$, $F = 3$), and blue-detuned blue MOT (at the D_1 or D_2 line depending on the configuration) beams, respectively. All these beams are switched on/off using acousto-optic modulators (AOMs). Each beam is further divided into three beams, overlapped, copropagated, made circularly polarized using dual $\lambda/4$ wave plates, expanded to a diameter of 25 mm, sent to the MOT chamber, and retroreflected back using a dual $\lambda/4$ wave plate and mirror. In each arm, the polarizations of L_1 and L_3 are the same, and L_2 and L_4 are the same but orthogonal to L_1 and L_3.

Atomic vapor is introduced into the MOT chamber by passing 2.15 A current to the dispenser (AlfaSource AS-Rb-0090-2C). First, the IR MOT is loaded for 2 s at the quadruple magnetic field (B') of 12.5 G/cm by switching on L_1 (power 50 mW and detuning -10 MHz from the $5S_{1/2}$, $F = 2 \rightarrow 5P_{3/2}$, $F = 3$ transition) and L_2 (power $P_{1\rightarrow2} = 33$ mW and detuning $\Delta_{1\rightarrow2}/2\pi = +40$ MHz from the $5S_{1/2}$, $F = 1 \rightarrow 5P_{3/2}$, $F = 2$) transition. The power of the L_1 is lowered by five times and is kept there for 4 ms to lower the temperature. The number of atoms N in the IR MOT is $\sim 1.3 \times 10^8$ and the temperature T is ~ 2 mK. Then it is transferred to the red-detuned blue MOT by switching off the L_1 beam and switching on the L_3 beam (power 26 mW and detuning -7 MHz from the $5S_{1/2}$, $F = 2 \rightarrow 6P_{3/2}$, $F = 3$ transition). After 4 ms, the power of the L_3 beam is reduced to 10 mW and detuning is ramped to $\Delta_{2\rightarrow3}/2\pi = -3$ MHz in 5 ms. After 20 ms of hold time, L_2, L_3, and B' are switched off. N and T are measured from the time-of-flight (TOF) method using absorption imaging at the $5S_{1/2}$, $F = 2 \rightarrow 5P_{3/2}$, $F = 3$ transition on a complementary metal-oxide-semiconductor (CMOS) camera with an exposure time of 100 μs.

IV. RESULTS AND DISCUSSION

We first study the effect of the orthogonally polarized IR repumper laser ($F_g = 1 \rightarrow F_e = 2$) on the IR MOT by changing the power ($P_{1\rightarrow2}$) at $\Delta_{1\rightarrow2}/2\pi = +40$ MHz. We observe that with an increase in $P_{1\rightarrow2}$ from 0.5 to 33 mW, T of the IR MOT increases from 1 to 2 mK. N also increases and saturates to 1.3×10^8. We then vary $\Delta_{1\rightarrow2}/2\pi$ from -20 to $+40$ MHz at $P_{1\rightarrow2} = 33$ mW. We observe no significant change in N and T. This is because the IR MOT laser is driving a closed transition and only a small fraction of atoms are lost due to off-resonant excitation.

Now, we study the effect of IR repumper on the red-detuned blue MOT. As the blue transition is open with a poor branching ratio, atoms decay continuously to the lower ground state, $F_g = 1$. Figures 2(b) and 2(c) show the variation of the T with $P_{1\rightarrow2}$ and $\Delta_{1\rightarrow2}/2\pi$ respectively for the configuration shown in Fig. 2(a). Here, the L_3 is at -3 MHz detuned to the $5S_{1/2}$, $F = 2 \rightarrow 6P_{3/2}$, $F = 3$ transition. First, the repumper laser is kept at $+40$ MHz detuned to the $F_g = 1 \rightarrow F_e = 2$ transition (which is also a type-I transition), and the power of the repumper laser is varied. We observe that with an increase in $P_{1\rightarrow2}$ from 5 to 30 mW, T decreases from 80 to 65 μK as shown in Fig. 2(b) by solid blue circle points. This is opposite to the case when the repumper laser is red detuned. When $\Delta_{1\rightarrow2}/2\pi = -5$ MHz, T increases from 90 to 105 μK as shown by the open red circle points in Fig. 2(b). In both the cases, N increases with the increase in $P_{1\rightarrow2}$ and then saturates to 1.1×10^8.

Next, we study the behavior of the red-detuned blue MOT with the detuning of the repumper laser $\Delta_{1\rightarrow2}/2\pi$ at three different powers, 10, 20, and 33.4 mW, as shown in Fig. 2(c) by the open green diamond, solid yellow triangle, and solid blue circle points, respectively. When $\Delta_{1\rightarrow2}/2\pi$ is varied from -20 to $+40$ MHz at $P_{1\rightarrow2} = 33.4$ mW, T decreases from 120 to 75 μK and then saturates. A similar pattern is observed at $P_{1\rightarrow2} = 10$ and 20 mW. We observe that blue-detuned laser cooling works even at a type-I transition and the blue-detuned repumper laser helps the narrow-line MOT at the blue transition to reach a lower temperature than the red-detuned repumper laser.

The same study is done for the configuration shown in Fig. 3(a), where the repumper laser is -5.2 MHz red detuned to the $F_g = 1 \rightarrow F_e = 1$ transition, which is a type-II transition. Similar to the previous case, T increases from 120 to 150 μK when the power of the repumper laser ($P_{1\rightarrow1}$) is

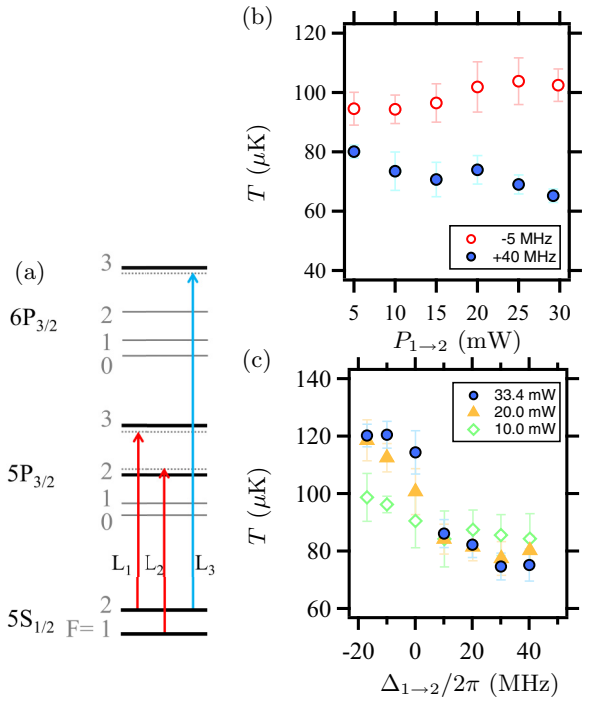

FIG. 2. Effect of the repumper laser, L_2 ($F_g = 1 \rightarrow F_e = 2$). (a) Relevant energy levels. (b) Temperature vs power of the repumper laser when $\Delta_{1\rightarrow2}/2\pi = +40$ MHz (solid blue circle) and -5 MHz (open red circle). (c) Temperature vs detuning of the repumper laser when $P_{1\rightarrow2} = 10$ mW (open green diamond), 20 mW (solid yellow triangle), and 33.4 mW (solid blue circle). L_1 is switched off.

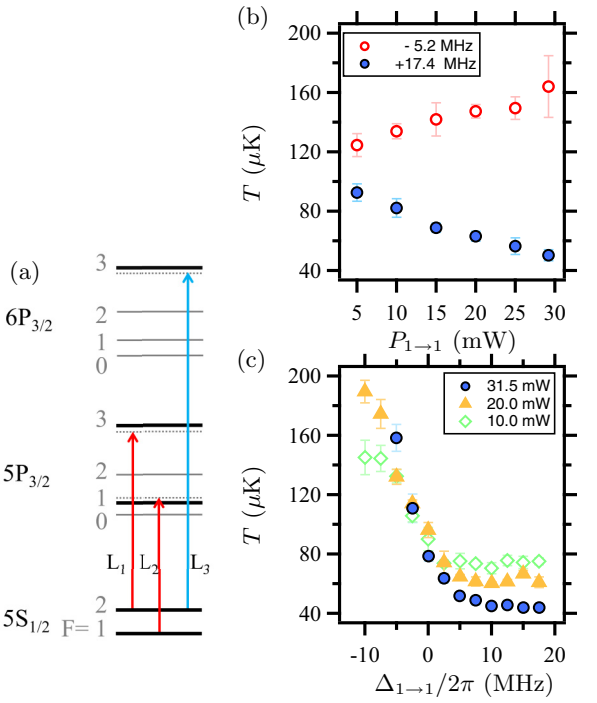

FIG. 3. Effect of the repumper laser, L_2 ($F_g = 1 \rightarrow F_e = 1$). (a) Relevant energy levels. (b) Temperature vs power of the repumper laser when $\Delta_{1\rightarrow1}/2\pi = +17.4$ MHz (solid blue circle) and -5.2 MHz (open red circle). (c) Temperature vs detuning of the repumper laser when $P_{1\rightarrow1} = 10$ mW (open green diamond), 20 mW (solid yellow triangle), and 31.5 mW (solid blue circle). L_1 is switched off.

increased from 5 to 30 mW [as shown in red in Fig. 3(b)]. In the blue-detuned repumper laser configuration, i.e., when $\Delta_{1\rightarrow1}/2\pi = +17.4$ MHz, T shows a decreasing trend from 90 to 44 μK with an increase in $P_{1\rightarrow1}$ from 5 to 30 mW. In both the cases, N increases with $P_{1\rightarrow1}$ and then saturates to 1.1×10^8.

We study the effect of repumper laser detuning ($\Delta_{1\rightarrow1}/2\pi$) on the blue MOT at three different powers, 10, 20, and 31.5 mW [as shown in Fig. 3(b) by the open green diamond, solid yellow triangle, and solid blue circle points, respectively]. At $P_{1\rightarrow1} = 31.5$ mW, T decreases from >200 to 44 μK and reaches saturation as the $\Delta_{1\rightarrow1}/2\pi$ is changed from -10 to $+17$ MHz. A similar trend is observed when $P_{1\rightarrow1} = 10$ and 20 mW, but T saturates to a higher value.

For completeness, we also study other configurations of the red-detuned as well as blue-detuned blue MOT, and the minimum temperature achieved at different configurations is summarized in Table I. The blue-detuned blue beams are generated by switching off the L_3 beams and switching on the L_4 beams. Additionally, the magnetic field is increased to 45 G/cm. The minimum temperatures of the blue MOT is 24 μK in the D_1 MOT using the $5S_{1/2}, F = 2 \rightarrow 6P_{1/2}, F = 2$ transition, and 31 μK in the D_2 MOT using the $5S_{1/2}, F = 2 \rightarrow 6P_{3/2}, F = 2$ transition. Unlike in Ref. [25], we have observed an almost spherical shape of the atomic cloud with a Gaussian distribution of atoms in all different configurations of the MOTs.

The temperature for the blue-detuned MOT will be determined by the width of the multiphoton transparency window. For the case of $F_g = 1 \leftrightarrow F_e = 1$ with counterpropagating σ^+ and σ^- laser beams, there is one V system (F_e; $m_F = -1 \leftrightarrow F_g$; $m_F = 0 \leftrightarrow F_e$; $m_F = +1$) and one Λ system (F_g; $m_F = -1 \leftrightarrow F_e$; $m_F = 0 \leftrightarrow F_g$; $m_F = +1$). In the steady state, the population will be redistributed, and only two sublevels, F_g; $m_F = +1$ and F_g; $m_F = -1$, will be populated, hence a Λ

TABLE I. Temperature of the different MOTs. Detuning ($\Delta/2\pi$ in MHz) of each laser from its corresponding transition is shown. The IR repumper laser is driving the $5S_{1/2}, F = 1 \rightarrow 5P_{3/2}, F = X$ transition, where $X = 1$ or 2. The blue MOT laser is driving the $5S_{1/2}$, $F = 2 \rightarrow 6P_{3/2(1/2)}$, $F = X$ transition for the $D_{2(1)}$ MOT, where $X = 1$, 2, or 3.

	IR repumper		Blue MOT		T
Case	Transition	$\Delta/2\pi$	Transition	$\Delta/2\pi$	(μK)
1	$1 \rightarrow 2$	$+40$	$D_2, 2 \rightarrow 3$	-3	65 ± 2
2	$1 \rightarrow 1$	$+17$	$D_2, 2 \rightarrow 3$	-3	44 ± 2
3	$1 \rightarrow 1$	$+17$	$D_2, 2 \rightarrow 3$	$+2$	53 ± 2
4	$1 \rightarrow 1$	$+14$	$D_2, 2 \rightarrow 2$	-2.5	32 ± 1
5	$1 \rightarrow 1$	$+14$	$D_2, 2 \rightarrow 2$	$+5$	31 ± 1
6	$1 \rightarrow 1$	$+14$	$D_1, 2 \rightarrow 2$	-2	40 ± 1
7	$1 \rightarrow 1$	$+14$	$D_1, 2 \rightarrow 2$	$+5$	24 ± 1
8	$1 \rightarrow 1$	$+14$	$D_1, 2 \rightarrow 1$	-2	61 ± 2

system will be formed. The width of the transparency window will be subnatural and determined by the decoherence rate of the ground-state magnetic sublevels $m_F = +1$ and $m_F = -1$ and the power broadening by the lasers.

For the case of $F_g = 1 \to F_e = 2$ with counterpropagating σ^+ and σ^- lasers, there is one V system (F_e; $m_F = -1 \leftrightarrow F_g$; $m_F = 0 \leftrightarrow F_e$; $m_F = +1$) and one W system (F_e; $m_F = -2 \leftrightarrow F_g$; $m_F = -1 \leftrightarrow F_e$; $m_F = 0 \leftrightarrow F_g$; $m_F = +1 \leftrightarrow F_e$; $m_F = +2$). The W system can be approximated as an impure Λ system. The impurity is quantified by the population in the $F_e : m_F = +2$ and $F_e : m_F = -2$ states. The linewidth of the transparency window will be approximated as $\sim\Omega^2\Gamma/(\Gamma^2 + \Delta^2)$. Therefore, the width of the transparency window will be narrower in the case of $F_g = 1 \to F_e = 1$ compared to $F_g = 1 \to F_e = 2$. Hence, blue-detuned cooling at $F_g = 1 \leftrightarrow F_e = 1$ will be more effective compared to the $F_g = 1 \leftrightarrow F_e = 2$ transition since the former is a pure Λ system. As a result, the second case (65 ± 2 μK) exhibits a higher temperature compared to the first case (44 ± 2 μK). Overall, the blue-detuned cooling is more efficient for the case $F_g \geqslant F_e$ than $F_g < F_e$ because, in the steady state, $F_g \geqslant F_e$ forms one or multiple Λ systems, whereas $F_g < F_e$ forms one or multiple W systems or WV systems.

The fourth and fifth cases yield similar temperatures but lower than the second case. This is because the blue transition $F_g = 2 \to F_e = 2$ populates the $F_g = 1$ state more compared to the $F_g = 2 \to F_e = 3$ transition, as the $F_e = 2$ can also directly decay to the $F_g = 1$ state, leading to more cooling by the repumper laser. The D_1 blue transition exhibits a higher temperature as it is a weaker transition and populates fewer atoms in the $F_g = 1$ state. In the seventh case, the temperature is lower because the number of atoms in the MOT decreases by a factor of 2.

V. CONCLUSION

In summary, we observe that STC plays a crucial role in laser cooling in the sub-Doppler regime. Prior to this work, it was known that there is no sub-Doppler cooling with blue-detuned lasers in a type-I transition. In this work, we show that it is possible to achieve cooling with blue-detuned lasers but in the absence of STC. As STC is very sensitive to stray magnetic fields, we observe blue-detuned cooling even in a type-I transition in MOT. For completeness, we also explore various combinations for the effectiveness of blue-detuned laser cooling in both type-I and type-II MOT configurations, achieving temperatures as low as 24 μK in the D_1 MOT and 31 μK in the D_2 MOT.

ACKNOWLEDGMENTS

The authors are grateful to Prof. T. N. Dey for fruitful discussions. R.C.D. acknowledges the Ministry of Education, Government of India, for the Prime Minister's Research Fellowship (PMRF), and K.P. acknowledges funding from DST through Grant No. DST/ICPS/QuST/Theme-3/2019.

APPENDIX: DENSITY MATRIX EQUATIONS

The equations [excluding Eqs. (3)–(5)] obtained using the density matrix analysis for the eight-level system are presented below:

$$\dot{\rho}_{11} = -\frac{i}{2}\Omega\left(\rho_{41} + \frac{1}{\sqrt{6}}\rho_{61}\right) + \text{H.c.} + \Gamma\left(\rho_{44} + \frac{1}{2}\rho_{55} + \frac{1}{6}\rho_{66}\right),$$

$$\dot{\rho}_{22} = -\frac{i}{2\sqrt{2}}\Omega(\rho_{52} + \rho_{72}) + \text{H.c.} + \Gamma\left(\frac{1}{2}\rho_{55} + \frac{2}{3}\rho_{66} + \frac{1}{2}\rho_{77}\right),$$

$$\dot{\rho}_{33} = -\frac{i}{2}\Omega\left(\frac{1}{\sqrt{6}}\rho_{63} + \rho_{83}\right) + \text{H.c.} + \Gamma\left(\frac{1}{6}\rho_{66} + \frac{1}{2}\rho_{77} + \rho_{88}\right),$$

$$\dot{\rho}_{44} = \frac{i}{2}\Omega\rho_{41} + \text{H.c.} - \Gamma\rho_{44},$$

$$\dot{\rho}_{55} = \frac{i}{2\sqrt{2}}\Omega\rho_{52} + \text{H.c.} - \Gamma\rho_{55},$$

$$\dot{\rho}_{66} = \frac{i}{2\sqrt{6}}\Omega(\rho_{61} + \rho_{63}) + \text{H.c.} - \Gamma\rho_{66},$$

$$\dot{\rho}_{77} = \frac{i}{2\sqrt{2}}\Omega\rho_{72} + \text{H.c.} - \Gamma\rho_{77},$$

$$\dot{\rho}_{88} = \frac{i}{2}\Omega\rho_{83} + \text{H.c.} - \Gamma\rho_{88},$$

$$\dot{\rho}_{14} = \frac{i}{2}\Omega\left(\rho_{11} - \rho_{44} - \frac{1}{\sqrt{6}}\rho_{64}\right) - i\,(\Delta - kv)\rho_{14} - \frac{1}{2}\Gamma\rho_{14},$$

$$\dot{\rho}_{15} = \frac{i}{2}\Omega\left(\frac{1}{\sqrt{2}}\rho_{12} - \rho_{45} - \frac{1}{\sqrt{6}}\rho_{65}\right) - i\,(\Delta - kv)\rho_{15} - \frac{1}{2}\Gamma\rho_{15},$$

$$\dot{\rho}_{16} = \frac{i}{2}\Omega\left(\frac{1}{\sqrt{6}}\rho_{11} + \frac{1}{\sqrt{6}}\rho_{13} - \rho_{46} - \frac{1}{\sqrt{6}}\rho_{66}\right) - i\,(\Delta + kv)\rho_{16} - \frac{1}{2}\Gamma\rho_{16},$$

$$\dot{\rho}_{17} = \frac{i}{2}\Omega\left(\frac{1}{\sqrt{2}}\rho_{12} - \rho_{47} - \frac{1}{\sqrt{6}}\rho_{67}\right) - i\,(\Delta + kv)\rho_{17} - \frac{1}{2}\Gamma\rho_{17},$$

$$\dot{\rho}_{18} = \frac{i}{2}\Omega\left(\rho_{13} - \rho_{48} - \frac{1}{\sqrt{6}}\rho_{68}\right) - i\,(\Delta + 3kv)\rho_{18} - \frac{1}{2}\Gamma\rho_{18},$$

$$\dot{\rho}_{24} = \frac{i}{2}\Omega\left(\rho_{21} - \frac{1}{\sqrt{2}}\rho_{54} - \frac{1}{\sqrt{2}}\rho_{74}\right) - i\,(\Delta - kv)\rho_{24} - \frac{1}{2}\Gamma\rho_{24},$$

$$\dot{\rho}_{25} = \frac{i}{2\sqrt{2}}\Omega(\rho_{22} - \rho_{55} - \rho_{75}) - i(\Delta - kv)\rho_{25} - \frac{1}{2}\Gamma\rho_{25},$$

$$\dot{\rho}_{26} = \frac{i}{2}\Omega\left(\frac{1}{\sqrt{6}}\rho_{21} + \frac{1}{\sqrt{6}}\rho_{23} - \frac{1}{\sqrt{2}}\rho_{56} - \frac{1}{\sqrt{2}}\rho_{76}\right) - i(\Delta + kv)\rho_{26} - \frac{1}{2}\Gamma\rho_{26},$$

$$\dot{\rho}_{27} = \frac{i}{2\sqrt{2}}\Omega(\rho_{22} - \rho_{57} - \rho_{77}) - i(\Delta + kv)\rho_{27} - \frac{1}{2}\Gamma\rho_{27},$$

$$\dot{\rho}_{28} = \frac{i}{2}\Omega\left(\rho_{23} - \frac{1}{\sqrt{2}}\rho_{58} - \frac{1}{\sqrt{2}}\rho_{78}\right) - i(\Delta + 3kv)\rho_{28} - \frac{1}{2}\Gamma\rho_{28},$$

$$\dot{\rho}_{34} = \frac{i}{2}\Omega\left(\rho_{31} - \frac{1}{\sqrt{6}}\rho_{64} - \rho_{84}\right) - i(\Delta - 3kv)\rho_{34} - \frac{1}{2}\Gamma\rho_{34},$$

$$\dot{\rho}_{35} = \frac{i}{2}\Omega\left(\frac{1}{\sqrt{2}}\rho_{32} - \frac{1}{\sqrt{6}}\rho_{65} - \rho_{85}\right) - i(\Delta - 3kv)\rho_{35} - \frac{1}{2}\Gamma\rho_{35},$$

$$\dot{\rho}_{36} = \frac{i}{2}\Omega\left(\frac{1}{\sqrt{6}}\rho_{31} + \frac{1}{\sqrt{6}}\rho_{33} - \frac{1}{\sqrt{6}}\rho_{66} - \rho_{86}\right) - i(\Delta - kv)\rho_{36} - \frac{1}{2}\Gamma\rho_{36},$$

$$\dot{\rho}_{37} = \frac{i}{2}\Omega\left(\frac{1}{\sqrt{2}}\rho_{32} - \frac{1}{\sqrt{6}}\rho_{67} - \rho_{87}\right) - i(\Delta - kv)\rho_{37} - \frac{1}{2}\Gamma\rho_{37},$$

$$\dot{\rho}_{38} = \frac{i}{2}\Omega\left(\rho_{33} - \frac{1}{\sqrt{6}}\rho_{68} - \rho_{88}\right) - i(\Delta + kv)\rho_{38} - \frac{1}{2}\Gamma\rho_{38},$$

$$\dot{\rho}_{45} = \frac{i}{2\sqrt{2}}\Omega\rho_{42} - \frac{i}{2}\Omega\rho_{15} - \Gamma\rho_{45},$$

$$\dot{\rho}_{46} = \frac{i}{2\sqrt{6}}\Omega(\rho_{41} + \rho_{43}) - \frac{i}{2}\Omega\rho_{16} - 2ikv\rho_{46} - \Gamma\rho_{46},$$

$$\dot{\rho}_{47} = \frac{i}{2\sqrt{2}}\Omega\rho_{42} - \frac{i}{2}\Omega\rho_{17} - 2ikv\rho_{47} - \Gamma\rho_{47},$$

$$\dot{\rho}_{48} = \frac{i}{2}\Omega\rho_{43} - \frac{i}{2}\Omega\rho_{18} - 4ikv\rho_{48} - \Gamma\rho_{48},$$

$$\dot{\rho}_{56} = \frac{i}{2\sqrt{6}}\Omega(\rho_{51} + \rho_{53}) - \frac{i}{2\sqrt{2}}\Omega\rho_{26} - 2ikv\rho_{56} - \Gamma\rho_{56},$$

$$\dot{\rho}_{57} = \frac{i}{2\sqrt{2}}\Omega(\rho_{52} - \rho_{27}) - 2ikv\rho_{57} - \Gamma\rho_{57},$$

$$\dot{\rho}_{58} = \frac{i}{2}\Omega\left(\rho_{53} - \frac{1}{\sqrt{2}}\rho_{28}\right) - 4ikv\rho_{58} - \Gamma\rho_{58},$$

$$\dot{\rho}_{67} = \frac{i}{2\sqrt{2}}\Omega\rho_{62} - \frac{i}{2\sqrt{6}}\Omega(\rho_{37} + \rho_{17}) - \Gamma\rho_{67},$$

$$\dot{\rho}_{68} = \frac{i}{2}\Omega\rho_{63} - \frac{i}{2\sqrt{6}}\Omega(\rho_{38} + \rho_{18}) - 2ikv\rho_{68} - \Gamma\rho_{68},$$

$$\dot{\rho}_{78} = \frac{i}{2}\Omega\rho_{73} - \frac{i}{2\sqrt{2}}\Omega\rho_{28} - 2ikv\rho_{78} - \Gamma\rho_{78}.$$

[1] R. Finkelstein, S. Bali, O. Firstenberg, and I. Novikova, A practical guide to electromagnetically induced transparency in atomic vapor, New J. Phys. **25**, 035001 (2023).

[2] S. E. Harris, J. E. Field, and A. Imamoğlu, Nonlinear optical processes using electromagnetically induced transparency, Phys. Rev. Lett. **64**, 1107 (1990).

[3] K. Pandey, Role of different types of subsystems in a doubly driven Λ system in ^{87}Rb, Phys. Rev. A **87**, 043838 (2013).

[4] A. Lezama, S. Barreiro, and A. M. Akulshin, Electromagnetically induced absorption, Phys. Rev. A **59**, 4732 (1999).

[5] A. V. Taichenachev, A. M. Tumaikin, and V. I. Yudin, Electromagnetically induced absorption in a four-state system, Phys. Rev. A **61**, 011802(R) (1999).

[6] H. R. Gray, R. M. Whitley, and C. R. Stroud, Coherent trapping of atomic populations, Opt. Lett. **3**, 218 (1978).

[7] J. Vanier, Atomic clocks based on coherent population trapping: A review, Appl. Phys. B **81**, 421 (2005).

[8] S. Menon and G. S. Agarwal, Effects of spontaneously generated coherence on the pump-probe response of a Λ system, Phys. Rev. A **57**, 4014 (1998).

[9] J. Javanainen, Effect of state superpositions created by spontaneous emission on laser-driven transitions, Europhys. Lett. **17**, 407 (1992).

[10] P. R. Berman, Spontaneously generated coherence and dark states, Phys. Rev. A **72**, 035801 (2005).

[11] A. V. Taichenachev, A. M. Tumaikin, and V. I. Yudin, On the spontaneous-coherence-transfer-induced sign change of a sub-natural-width nonlinear resonance, J. Exp. Theor. Phys. Lett. **69**, 819 (1999).

[12] W.-H. Xu, J.-H. Wu, and J.-Y. Gao, Transient response in a three-level V system with spontaneously generated coherence, Opt. Commun. **215**, 345 (2003).

[13] E. Paspalakis, S.-Q. Gong, and P. L. Knight, Spontaneous emission-induced coherent effects in absorption and dispersion of a V-type three-level atom, Opt. Commun. **152**, 293 (1998).

[14] D. Wang and Y. Zheng, Quantum interference in a four-level system of a ^{87}Rb atom: Effects of spontaneously generated coherence, Phys. Rev. A **83**, 013810 (2011).

[15] Z. Song, Y. Peng, Z.-D. Sun, and Y. Zheng, Spontaneously generated coherence in a Rb atom via photon counting statistics, J. Phys. B: At. Mol. Opt. Phys. **49**, 015001 (2016).

[16] A. Silatan, M. Ghaderi GoranAbad, and M. Mahmoudi, Optical limiting via spontaneously generated coherence, Sci. Rep. **13**, 364 (2023).

[17] V. Entin, I. Ryabtsev, A. Boguslavsky, and Y. Brzhazovsky, Laser spectroscopy of spontaneous coherence transfer and optically induced polarization rotation in ^{87}Rb, Opt. Commun. **207**, 201 (2002).

[18] J. Dalibard and C. Cohen-Tannoudji, Laser cooling below the Doppler limit by polarization gradients: Simple theoretical models, J. Opt. Soc. Am. B **6**, 2023 (1989).

[19] J. A. Devlin and M. R. Tarbutt, Three-dimensional Doppler, polarization-gradient, and magneto-optical forces for atoms and molecules with dark states, New J. Phys. **18**, 123017 (2016).

[20] J. P. McGilligan, P. F. Griffin, R. Elvin, S. J. Ingleby, E. Riis, and A. S. Arnold, Grating chips for quantum technologies, Sci. Rep. **7**, 384 (2017).

[21] Y.-S. Chin, M. Steiner, and C. Kurtsiefer, Polarization gradient cooling of single atoms in optical dipole traps, Phys. Rev. A **96**, 033406 (2017).

[22] M. Walhout, U. Sterr, and S. L. Rolston, Magnetic inhibition of polarization-gradient laser cooling in $\sigma_+ - \sigma_-$ optical molasses, Phys. Rev. A **54**, 2275 (1996).

[23] M. Walhout, J. Dalibard, S. L. Rolston, and W. D. Phillips, σ_+–σ_- optical molasses in a longitudinal magnetic field, J. Opt. Soc. Am. B **9**, 1997 (1992).

[24] K. N. Jarvis, J. A. Devlin, T. E. Wall, B. E. Sauer, and M. R. Tarbutt, Blue-detuned magneto-optical trap, Phys. Rev. Lett. **120**, 083201 (2018).

[25] K. N. Jarvis, B. E. Sauer, and M. R. Tarbutt, Characteristics of unconventional Rb magneto-optical traps, Phys. Rev. A **98**, 043432 (2018).

[26] B. Piest, V. Vollenkemper, J. Böhm, A. Herbst, and E. M. Rasel, Red- and blue-detuned magneto-optical trapping with liquid crystal variable retarders, Rev. Sci. Instrum. **93**, 023202 (2022).

[27] T. Grünzweig, A. Hilliard, M. McGovern, and M. F. Andersen, Near-deterministic preparation of a single atom in an optical microtrap, Nat. Phys. **6**, 951 (2010).

[28] A. Jenkins, J. W. Lis, A. Senoo, W. F. McGrew, and A. M. Kaufman, Ytterbium nuclear-spin qubits in an optical tweezer array, Phys. Rev. X **12**, 021027 (2022).

[29] J. J. Burau, P. Aggarwal, K. Mehling, and J. Ye, Blue-detuned magneto-optical trap of molecules, Phys. Rev. Lett. **130**, 193401 (2023).

[30] S. Xu, R. Li, Y. Xia, M. Siercke, and S. Ospelkaus, Blue-detuned molecular magneto-optical trap schemes based on Bayesian optimization, Phys. Rev. A **108**, 033102 (2023).

[31] V. Jorapur, T. K. Langin, Q. Wang, G. Zheng, and D. DeMille, High density loading and collisional loss of laser-cooled molecules in an optical trap, Phys. Rev. Lett. **132**, 163403 (2024).

[32] S. J. Li, C. M. Holland, Y. Lu, and L. W. Cheuk, Blue-detuned magneto-optical trap of CaF molecules, Phys. Rev. Lett. **132**, 233402 (2024).

[33] C. Hallas, G. K. Li, N. B. Vilas, P. Robichaud, L. Anderegg, and J. M. Doyle, High compression blue-detuned magneto-optical trap of polyatomic molecules, arXiv:2404.03636.

[34] R. C. Das, D. Shylla, A. Bera, and K. Pandey, Narrow-line cooling of ^{87}Rb using $5S_{1/2} \rightarrow 6P_{3/2}$ open transition at 420 nm, J. Phys. B: At. Mol. Opt. Phys. **56**, 025301 (2023).

[35] R. Ding, A. Orozco, J. Lee, and N. Claussen, Narrow-linewidth laser cooling for rapid production of low-temperature atoms for high data-rate quantum sensing, LDRD Project No. 226345, Sandia National Laboratory Technical Report No. SAND2022-15828R, doi:10.2172/1898260 (2022).

[36] R. C. Das, T. Ravi, S. Khan, and K. Pandey, Continuous loading of a magneto-optical trap of Rb using a narrow transition, Phys. Rev. A **109**, 063107 (2024).

[37] P. M. Duarte, R. A. Hart, J. M. Hitchcock, T. A. Corcovilos, T.-L. Yang, A. Reed, and R. G. Hulet, All-optical production of a lithium quantum gas using narrow-line laser cooling, Phys. Rev. A **84**, 061406(R) (2011).

[38] J. Sebastian, C. Gross, K. Li, H. C. J. Gan, W. Li, and K. Dieckmann, Two-stage magneto-optical trapping and narrow-line cooling of ^{6}Li atoms to high phase-space density, Phys. Rev. A **90**, 033417 (2014).

[39] D. C. McKay, D. Jervis, D. J. Fine, J. W. Simpson-Porco, G. J. A. Edge, and J. H. Thywissen, Low-temperature high-density magneto-optical trapping of potassium using the open $4S \rightarrow 5P$ transition at 405 nm, Phys. Rev. A **84**, 063420 (2011).

[40] E. A. Curtis, C. W. Oates, and L. Hollberg, Quenched narrow-line laser cooling of ^{40}Ca to near the photon recoil limit, Phys. Rev. A **64**, 031403(R) (2001).

[41] E. A. Curtis, C. W. Oates, and L. Hollberg, Quenched narrow-line second- and third-stage laser cooling of ^{40}Ca, J. Opt. Soc. Am. B **20**, 977 (2003).

[42] H. Katori, T. Ido, Y. Isoya, and M. Kuwata-Gonokami, Magneto-optical trapping and cooling of strontium atoms down to the photon recoil temperature, Phys. Rev. Lett. **82**, 1116 (1999).

[43] T. Yang, K. Pandey, M. S. Pramod, F. Leroux, C. C. Kwong, E. Hajiyev, Z. Y. Chia, B. Fang, and D. Wilkowski, A high flux source of cold strontium atoms, Eur. Phys. J. D **69**, 226 (2015).

[44] T. Kuwamoto, K. Honda, Y. Takahashi, and T. Yabuzaki, Magneto-optical trapping of Yb atoms using an intercombination transition, Phys. Rev. A **60**, R745(R) (1999).

[45] K. Pandey, K. D. Rathod, A. K. Singh, and V. Natarajan, Atomic fountain of laser-cooled Yb atoms for precision measurements, Phys. Rev. A **82**, 043429 (2010).

[46] M. Lu, S. H. Youn, and B. L. Lev, Spectroscopy of a narrow-line laser-cooling transition in atomic dysprosium, Phys. Rev. A **83**, 012510 (2011).

[47] T. Maier, H. Kadau, M. Schmitt, A. Griesmaier, and T. Pfau, Narrow-line magneto-optical trap for dysprosium atoms, Opt. Lett. **39**, 3138 (2014).

[48] A. J. Berglund, J. L. Hanssen, and J. J. McClelland, Narrow-line magneto-optical cooling and trapping of strongly magnetic atoms, Phys. Rev. Lett. **100**, 113002 (2008).

[49] A. Frisch, K. Aikawa, M. Mark, A. Rietzler, J. Schindler, E. Zupanič, R. Grimm, and F. Ferlaino, Narrow-line magneto-optical trap for erbium, Phys. Rev. A **85**, 051401(R) (2012).

[50] B. Seo, P. Chen, Z. Chen, W. Yuan, M. Huang, S. Du, and G.-B. Jo, Efficient production of a narrow-line erbium magneto-optical trap with two-stage slowing, Phys. Rev. A **102**, 013319 (2020).

[51] A. Yamaguchi, M. S. Safronova, K. Gibble, and H. Katori, Narrow-line cooling and determination of the magic wavelength of Cd, Phys. Rev. Lett. **123**, 113201 (2019).

[52] Y. Miyazawa, R. Inoue, H. Matsui, K. Takanashi, and M. Kozuma, Narrow-line magneto-optical trap for europium, Phys. Rev. A **103**, 053122 (2021).

[53] S. Chang and V. Minogin, Density-matrix approach to dynamics of multilevel atoms in laser fields, Phys. Rep. **365**, 65 (2002).

[54] R. C. Das, S. Khan, T. Ravi, and K. Pandey, Direct spectroscopy of rubidium using a narrow-line transition at 420 nm, Eur. Phys. J. D **78**, 40 (2024).